J Mater Sci (2006) 41:6647–6654
DOI 10.1007/s10853-006-0195-4

Multi-scale modeling of refractory woven fabric composites

Y. W. Kwon · D. H. Kim · T. Chu

Published online: 17 August 2006

Abstract Thermomechanical analysis of a refractory, woven fabric composite was conducted using a multi-scale analysis technique. The composite was made of carbons and ceramic materials. The fibers were made of carbons and the outer coating was made of a ceramic material. In order to reduce the thermal stress in the carbon fibers and the ceramic material caused by mismatch of coefficients of thermal expansion between the two materials, a graphitized carbon layer was introduced between the fiber and the ceramic coating. For the multi-scale analysis, a new analysis model was developed and used to bridge the micro-scale characteristics, i.e. the constituent material level such as carbon and ceramic materials, to the macro-scale behavior, i.e. the woven fabric composite level. Furthermore, finite element analyses were undertaken with discrete modeling of the representative fibers, coating, and the graphitized middle layers. Then, both multi-scale analytical and numerical results were compared. In this study, thermal stresses at the micro-level, i.e. in the fibers and coating materials, as well as effective thermomechanical properties of the refractory composites were computed using the multi-scale technique.

Y. W. Kwon (✉)
Department of Mechanical and Aeronautical Engineering,
Naval Postgraduate School, Monterey, CA 93943, USA
e-mail: ywkwon@nps.edu

D. H. Kim · T. Chu
Department of Mechanical Engineering and Energy Processes,
Southern Illinois University, Carbondale, IL 62901, USA

Introduction

As technology moves beyond its traditional boundary, there are more challenges to engineers and scientists. As an example, a hypersonic aircraft structure is subjected to a very high temperature, such as around 2000 °K, and a large thermal variation. For high temperature application, a thermal protection system is required. Carbon composites showed good structural properties at such very high temperatures, but they are not oxidation resistant. In order to prevent the carbon from being oxidized, ceramic coatings have been considered. However, mismatch of coefficient of thermal expansion (CTE) between the carbon fibers and the ceramic coating causes high thermal stress in the coating material. The high thermal stress level can yield cracking in the brittle coating, which results in failure of anti-oxidation protection to the carbon fibers. One way to relieve the high thermal stress in the coating was by introducing a weakly bonded layer between the carbon fiber and the ceramic coating so that the constraint due to CTE mismatch can be relaxed. The interlayer considered was a graphitized carbon layer generated through Chemical Vapor Infiltration (CVI) technique.

The objective of the present study was to develop a multi-scale technique to analyze a refractory woven fabric composite made of the carbon fibers, interlayers, and coating. Using the technique, we investigated the micro-level thermal stresses occurring in the constituent material level such as the fiber and the coating layer as well as to predict the effective material properties of a refractory woven fabric composite made of the fibers, interlayers, and coating.

For the multi-scale analysis, a series of analysis models were used to bridge the micro-scale characteristics (i.e. the constituent material level such as the fiber, interlayer, and

coating materials) to the macro-scale behavior (i.e. the woven fabric composite level). Furthermore, finite element analyses were undertaken with discrete modeling of the representative fibers, coating, and the graphitized middle layers. Then, both analytical and numerical results were compared. In addition, thermal stresses at the micro-level, i.e. in the fibers and coating materials, as well as effective thermomechanical properties of the refractory composites were computed using the multi-scale technique.

Thermal stresses in structures including composite structures have been extensively studied [1, 2]. Many of the studies [3–5] were macro-level analyses while some others [6–9] were micro-level analyses. Thermal stress occurring at the micro-level due to mismatch of CTEs in constituent materials of a composite played an important role in composite failure at the macro-level [5]. Therefore, calculation of micro-level thermal stress is critical to predict and present thermal stress failure in a composite. As a result, this paper investigated the micro-level thermal stress and effective thermomechanical properties of a refractory composite of woven fabric. The paper is organized as below: The next sections discuss the multi-scale modeling and the finite element modeling, respectively, for a refractory plain weave composite made of the fibers, interlayers, and coating. Then they are followed by results and discussion. Finally, conclusions are provided at the end.

Multi-scale analysis technique

First of all, a general multi-scale analysis technique for a composite structure, as sketched in Fig. 1, is described. Then, more detailed description for each scale level analysis for the present refractory composite is provided subsequently. The general multi-scale analysis technique spans from nano-scale to macro-scale as illustrated in the figure.

To initiate the multi-scale analysis, the nano-scale analysis is applied to atoms and/or molecules that make the composite material. For the nano-scale analysis, the molecular dynamics or discrete atomic model is utilized. From the nano-scale analysis, material properties of respective fibers and binding materials can be determined. These properties include strength and stiffness of the materials as well as their interfaces. Once these properties are obtained and their volume fractions to construct the unidirectional fibrous composite are provided, the micro-scale analysis using a unit-cell model is used to obtain the stiffness of the unidirectional fiber-reinforced composite geometry. The stiffness properties of the unidirectional composite are substituted into the macro-scale analysis along with the geometric data of the woven fabric composite to be analyzed. Another unit-cell model is used for the woven fabric composite to compute the effective stiffness of the woven-fabric lamina. Then, the lamina properties are used to calculate the laminated composite properties of a laminated composite structure using the lamination theory. Using those material properties, the finite element analysis is performed for a composite structure in order to compute the structural response under the given load, i.e. deformation, strains, stresses, etc. The processes so far complete one forward cycle of the multi-scale analysis in order to compute the effective thermomechanical properties of the final composite structure. The next set of processes described below is related to the backward cycle of the multi-scale analysis to close the loop of the multi-scale analysis in order to compute thermomechanical stresses in the constituent materials like the fibers and the binding materials.

The stresses and strains computed using the finite element analysis are decomposed into the stresses and strains at each woven-fabric layer of the composite structure. The latter stresses and strains are again utilized to calculate stresses and strains at the unidirectional composite level. Finally, the stresses and strains at the unidirectional composite level are decomposed into the stresses and strains at the fibers and the binding materials as sketched in Fig. 1. Then, the latter stresses and strains are applied to damage mechanics or failure criteria to determine whether there is any damage or failure at the constituent material level, such as fiber breakage, matrix cracking, and/or interface debonding. If there is a localized damage or failure, degraded material properties are computed using the damage mechanics with completion of one cycle of the multi-scale analysis. In the multi-scale analysis, progressive damage and failure of composite structures are described at the constituent material level so that physics-based damage or failure theories can be applied. In addition, such a damage or failure model simplifies various failure modes at the macro-level. For example, interlayer delamination, transverse matrix cracking, or fiber splitting can be explained in terms of matrix damage at different locations and directions.

For the present refractory composite analysis, only the micro-scale and macro-scale analyses were conducted as described later in this section. In other words, the fiber, interlayer, and coating materials were known for the multi-scale analysis. Hence, the micro-scale and macro-scale analysis models are described below:

Micro-scale model

Micro-scale models developed previously [5, 8, 10] did not address the middle layer and its weak-bonding characteristics, which is the key aspect of the current refractory composite. As a result, a new model is developed here to include the interlayer and its weak intra-layer bonding. The proposed model is a unit-cell model as sketched in Fig. 2

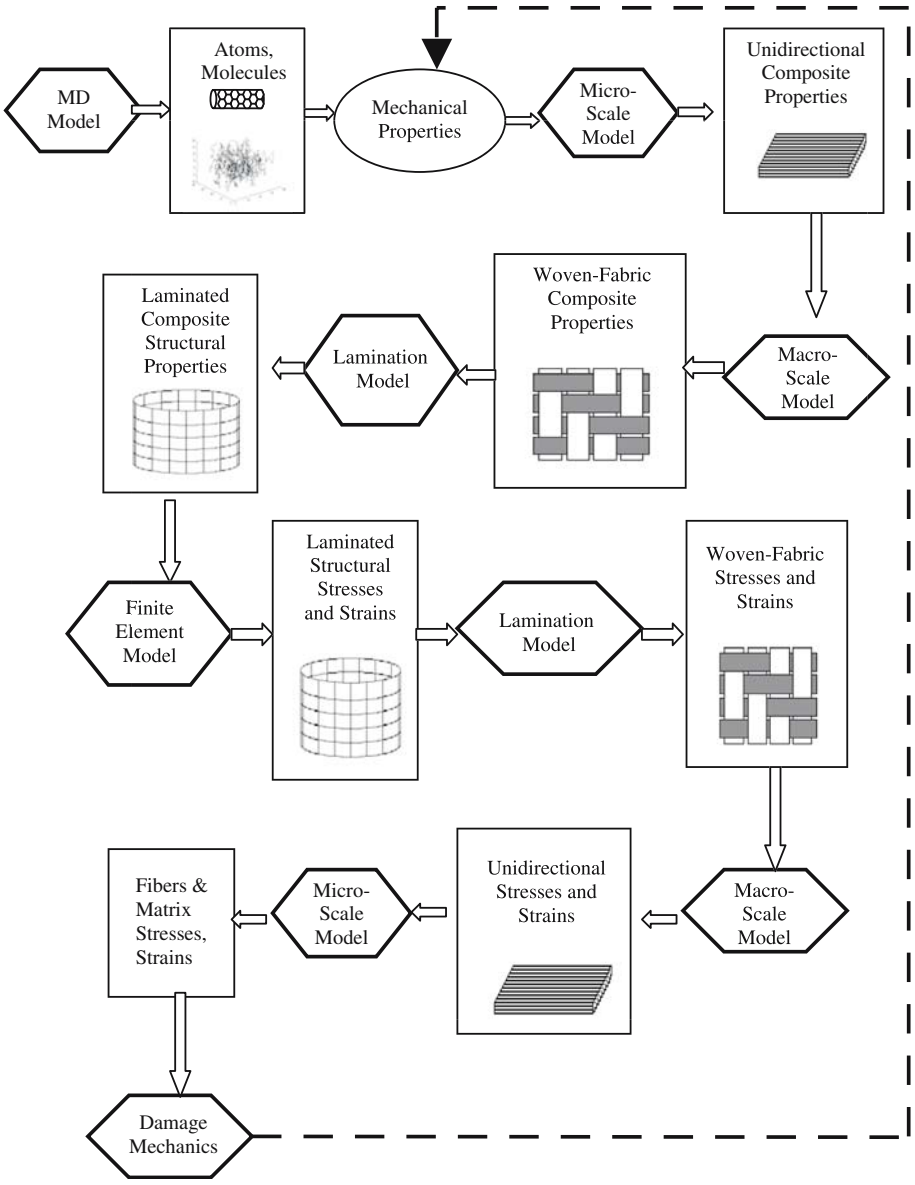

Fig. 1 Schematic diagram for multi-scale analysis of structures made of laminated woven fabric composites

where the x-axis is along the fiber orientation. The unit-cell model has 9 sub-cells with symmetries in planes x–y and x–z. Sub-cell 1 represents the fiber, sub-cells 2, 4, and 5 denote the CVI-layer, and sub-cells 3, 6, 7, 8, and 9 are the coating materials. The dimension of each sub-cell, a, b, c in the figure, is determined from the volume fraction of each material, i.e. the fiber, the bonding layer, and the coating. Let v_f, v_m, and v_c be the volume fraction of the fiber, the bonding layer, and the coating. Then, the geometric dimensions are computed as

$$a = \sqrt{v_f}, b = \sqrt{a^2 + v_m} - a, \quad c = 1 - a - b \tag{1}$$

The equilibrium between each sub-cell is given below:

$$\sigma_y^1 = \sigma_y^2, \sigma_y^2 = \sigma_y^3, \sigma_y^4 = \sigma_y^5, \sigma_y^5 = \sigma_y^6, \sigma_y^7 = \sigma_y^8, \sigma_y^8 = \sigma_y^9 \tag{2}$$

$$\sigma_z^1 = \sigma_z^4, \sigma_z^4 = \sigma_z^7, \sigma_z^2 = \sigma_z^5, \sigma_z^5 = \sigma_z^8, \sigma_z^3 = \sigma_z^6, \sigma_z^6 = \sigma_z^9 \tag{3}$$

where the subscript indicates the axis and the superscript is for the sub-cell. The first set of equations is for the equilibrium in the y-direction, and the second set is for the z-direction.

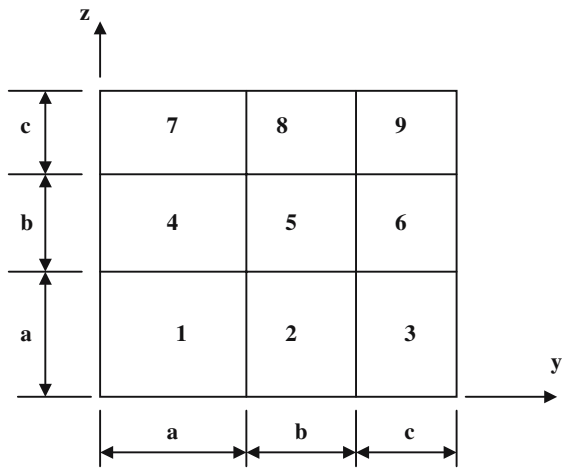

Fig. 2 Cross-sectional view of the unit-cell for a fibrous composite made of the fiber (sub-cell # 1), interlayer (sub-cell # 2, 4, 5), and coating (sub-cell # 3, 6, 7, 8, 9)

The deformation compatibility are written as

$$a\varepsilon_y^1 + b\varepsilon_y^2 + c\varepsilon_y^3 = a\varepsilon_y^4 + b\varepsilon_y^5 + c\varepsilon_y^6 = a\varepsilon_y^7 + b\varepsilon_y^8 + c\varepsilon_y^9 \quad (4)$$

$$a\varepsilon_z^1 + b\varepsilon_z^4 + c\varepsilon_z^7 = a\varepsilon_z^2 + b\varepsilon_z^5 + c\varepsilon_z^8 = a\varepsilon_z^3 + b\varepsilon_z^6 + c\varepsilon_z^9 \quad (5)$$

for the y- and z-direction, respectively. The deformation compatibility in the x-direction (i.e. fiber orientation) is given as below:

$$\varepsilon_x^2 = \varepsilon_x^5, \varepsilon_{\mathrm{x}}^4 = \varepsilon_x^5 \quad (6)$$

$$\varepsilon_x^3 = \varepsilon_x^6, \varepsilon_{\mathrm{x}}^6 = \varepsilon_x^9, \varepsilon_x^7 = \varepsilon_x^8, \varepsilon_{\mathrm{x}}^8 = \varepsilon_x^9 \quad (7)$$

These equations state that the bonding-layer and the coating layer have the same deformation along the fiber direction, respectively. If the fiber, bonding-layer, and coating layer are bonded together perfectly, there are two more equations as below:

$$\varepsilon_x^1 = \varepsilon_x^2, \varepsilon_{\mathrm{x}}^2 = \varepsilon_x^3 \quad (8)$$

On the other hand, if the fiber, bonding-layer, and coating layer are allowed to slide one another due to imperfect bonding, which was introduced intentionally in the present composite, Eq. (8) is no longer true. Instead, the relative movement should be included in deformation compatibility equations in the fiber's longitudinal direction as below:

$$\varepsilon_x^1 - \varepsilon_x^2 = \left(\alpha_x^1 - \alpha_x^2\right)\Delta\theta - \left(\frac{\mathrm{sgn}(\alpha_{\mathrm{x}}^1 - \alpha_{\mathrm{x}}^2)\tau^{1-2}}{aE_x^1} + \frac{\mathrm{sgn}(\alpha_{\mathrm{x}}^1 - \alpha_{\mathrm{x}}^2)\tau^{1-2}\mathrm{a} - \mathrm{sgn}(\alpha_{\mathrm{x}}^2 - \alpha_{\mathrm{x}}^3)\tau^{2-3}(\mathrm{a}+\mathrm{b})}{b(b+2a)E_x^2}\right) \quad (9a)$$

$$\varepsilon_x^2 - \varepsilon_x^3 = \left(\alpha_x^2 - \alpha_x^3\right)\Delta\theta - \left(\frac{-\mathrm{sgn}(\alpha_{\mathrm{x}}^1 - \alpha_{\mathrm{x}}^2)\tau^{1-2}\mathrm{a} + \mathrm{sgn}(\alpha_{\mathrm{x}}^2 - \alpha_{\mathrm{x}}^3)\tau^{2-3}(\mathrm{a}+\mathrm{b})}{b(b+2a)E_x^2} + \frac{\mathrm{sgn}(\alpha_{\mathrm{x}}^2 - \alpha_{\mathrm{x}}^3)\tau^{2-3}(\mathrm{a}+\mathrm{b})}{c(1+a+b)E_x^3}\right) \quad (9b)$$

Here, sgn( ) is the sign function such that

$$\mathrm{sgnx} = \begin{cases} -1 & : \mathrm{x}<0 \\ 0 & : \mathrm{x}=0 \\ 1 & : \mathrm{x}>0 \end{cases} \quad (10)$$

and α_x^i and E_x^i are the CTE and elastic modulus of the ith sub-cell in the x-axis. In addition, τ^{i-j} is the interface shear stress between the ith and jth sub-cells. $\Delta\theta$ is a temperature change. A uniform shear stress was assumed for the equations.

The unit-cell strain and stress are assumed to be the volume average of the sub-cell strains and stresses, respectively. That is,

$$\varepsilon_{ij}^{\mathrm{unit}} = \sum_{n=1}^{9} V^n \varepsilon_{ij}^n \ \ (i,j=1,\,2,\,3) \quad (11)$$

$$\sigma_{ij}^{\mathrm{unit}} = \sum_{n=1}^{9} V^n \sigma_{ij}^n \ \ (i,j=1,2,3) \quad (12)$$

Here, V^n is the volume fraction of the nth sub-cell. The constitutive equation for each sub-cell is expressed as

$$\varepsilon_{ij}^n = C_{ijkl}^n \sigma_{kl}^n + \alpha_{ij}^n \Delta\theta \ \ (i,j,k,1=1,2,3) \quad (13)$$

in which summation sign convention is applied only to the subscripts, k and l, but not to the superscript n. The same rule applies for the following derivation. Furthermore, C_{ijkl}^n and α_{ij}^n are the mechanical and thermal property tensors. Writing stresses in terms of strains yields

$$\sigma_{ij}^n = E_{ijkl}^n \varepsilon_{kl}^n - \tau_{ij}^n \quad (14)$$

in which

$$\tau_{ij}^n = E_{ijkl}^n \alpha_{kl}^n \Delta\theta \quad (15)$$

and E_{ijkl}^n is the inverse of C_{ijkl}^n. The unit-cell level stresses and strains are expressed as

$$\varepsilon_{ij}^{\mathrm{unit}} = C_{ijkl}^{\mathrm{unit}} \sigma_{kl}^{\mathrm{unit}} + \alpha_{ij}^{\mathrm{unit}} \Delta\theta \quad (16)$$

where C_{ijkl}^{unit} and $\alpha_{ij}^{\text{unit}}$ are the effective mechanical and thermal properties of the unidirectional composite. The algebraic manipulation of the above equations results in the matrix equation

$$[T]\{\varepsilon\} = \{f\} \tag{17}$$

in which $[T]$ is the matrix consisting of E_{ijkl}^{unit} and geometric data of the unit-cell, and $\{\epsilon\}$ is the vector containing sub-cell strains of the unit-cell module. In addition, vector $\{f\}$ has sub-vectors like

$$\{f\}^T = \left\{ \left\{\Delta\tau^{\text{unit}}\right\}^T \quad \{0\}^T \quad \left\{\varepsilon^{\text{unit}}\right\}^T \right\} \tag{18}$$

where $\left\{\Delta\tau^{\text{unit}}\right\}$ is vector containing components $\{\Delta\tau\}$. Pre-multiplication of the inverse of $[T]$ to the above equation yields

$$\{\varepsilon\} = [R_1]\{\Delta\tau\} + [R_2]\left\{\varepsilon^{\text{unit}}\right\} \tag{19}$$

Here,

$$[R] = [T]^{-1} = [\,[R_1] \quad [0] \quad [R_2]\,] \tag{20}$$

Equation (11) can be rewritten as

$$\left\{\sigma^{\text{unit}}\right\} = [V]\{\sigma\} \tag{21}$$

Substitution of sub-cell strains of Eq. (19) into Eq. (14), and subsequent substitution of the resultant expression into Eq. (21) yields the stress–strain relationship at the unit-cell level. Comparing the resultant expression to Eq. (16) gives the mathematical expressions for effective thermo-mechanical properties of the unidirectional composite as shown below:

$$\left[E^{\text{unit}}\right] = [V][E][R_2] \tag{22}$$

$$\left\{\alpha^{\text{unit}}\right\} = -\left[E^{\text{unit}}\right]^{-1}[V]([E][R_1]\{\Delta\tau\} - \{\tau\})\Big/\Delta\theta \tag{23}$$

The thermomechanical properties obtained from Eqs. (22) and (23) are used for the macro-scale analysis. For the present analysis, the plain woven fabric composite was considered.

The micro-thermal stresses can be computed as follows. Under a free, thermal deformation, the effective stresses vanish, and the unit-cell level strains are caused by the unit-cell level CTE's. Use of this condition along with Eqs. (14) and (19) yields the following expression for the micro-level thermal stresses, i.e. the thermal stresses in the fiber, bonding-layer, and coating materials.

$$\{\sigma\} = [E]\left([R_1]\{\Delta\tau\} + [R_2]\left\{\alpha^{\text{unit}}\right\}\Delta\theta\right) - \{\tau\} \tag{24}$$

Macro-scale model

The textile composite at the macro-scale can be classified as weaves, knits, and braids, etc. [11]. The preform under investigation is a woven fabric. The fabric also has different types of patterns such as plain weave, satin weave, 2/2-twill, etc. Among them, the plain weave was examined in this study. As a result, a unit-cell model for the plain weave composite was utilized. The model computes the effective thermomechanical properties of the plain weave using the materials properties obtained from the micro-scale analysis as described previously as well as the weaving geometry. In addition, the macro-scale unit-cell model decomposes the unit-cell level stresses and strains into the sub-cell level stresses and strains that are inputted into the micro-scale model so that micro-scale thermal stresses can be finally obtained.

A unit-cell for the plain weave, as shown in Fig. 3, was previously developed [9]. The same model could be utilized in the present study. As a result, the detailed discussion of the model was omitted here.

Finite element analysis models for composites

A detailed finite element analysis model was developed for the plain weave composite. The model consists of discrete representative fibers, interlayers, and the surrounding coating materials as seen in Figs. 4–6. The figures show representative fibers, interlayers, and the coating layer, separately for visual clarity, even though the finite element analysis considered the whole things together. Because modeling actual individual sizes of the fibers exceeds modern computational capabilities, only representative fibers were modeled for the composites. This simplification could capture the basic characteristics of the composite behavior [9].

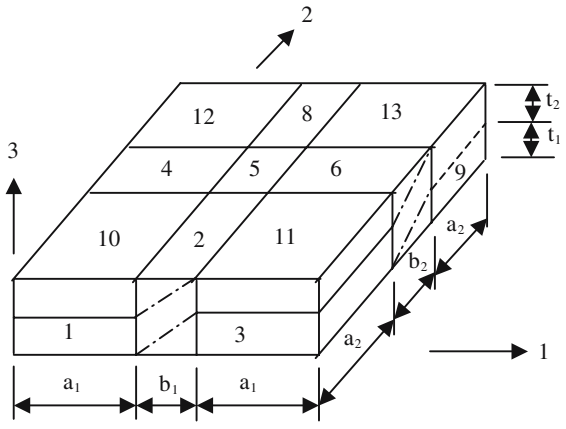

Fig. 3 Macro-scale unit-cell model for a plain weave composite

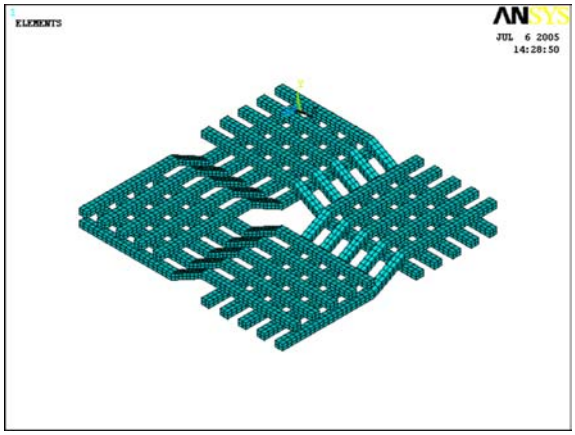

Fig. 4 Finite element analysis model for a plain weave composite showing only the representative fibers

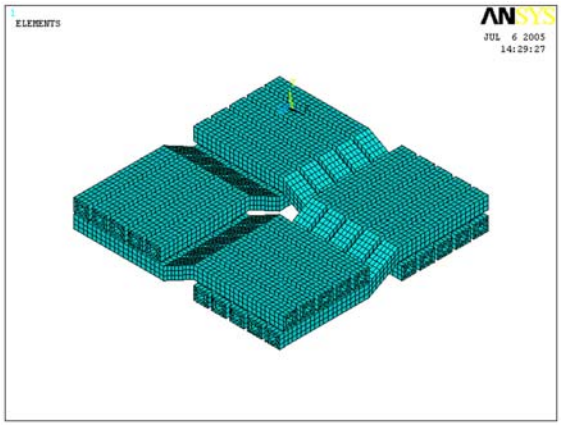

Fig. 5 Finite element analysis model for a plain weave composite showing only the interlayers

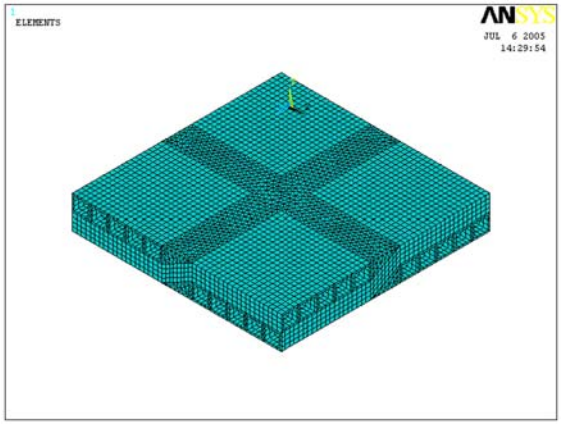

Fig. 6 Finite element analysis model for a plain weave composite showing only coating layer

Furthermore, another finite element modeling and analysis was conducted for the representative single fiber model as sketched in Fig. 7. The model considered a single fiber surrounded by the interlayer and the coating material. The results of the single fiber model were used to evaluate the results from the micro-scale analysis in terms of thermal stresses and mechanical properties.

In both finite element analyses described above, the interlayer was modeled in two different ways. The interlayer has weak bonding among its intra-layers, which can reduce thermal stresses caused by mismatch of CTE's among the constituent materials. As a result, such a weak bonding in the interlayer was considered as a very thin and soft material in the finite element model. Secondly, the weak bonding was neglected in order to examine the effect of the weak bonding in the interlayer on the thermal stresses. As a result, the two cases with or without weak bonding in the interlayer were compared.

Results and discussion

First of all, the representative single fiber model as sketched in Fig. 7 was analyzed using the unit-cell based micro-scale analysis as well as the detailed finite element analysis. The materials used in this study are provided below. The fiber has the modulus of 230 GPa and CTE of 9.74×10^{-6}/°C, respectively. The interlayer has the elastic modulus of 40 GPa and CTE of 5.0×10^{-6}/°C. The ceramic coating material has the elastic modulus of 400 GPa and CTE of 4.4×10^{-6}/°C. The volume fractions for the fiber, interlayer, and the coating are 0.39, 0.17, and 0.44, respectively.

For the weakly bonded inter-layer, the thermal stresses computed from the unit-cell model were 0.11 MPa in tension for the fiber and 0.11 MPa in compression for the coating per unit temperature change. The axisymmetric finite element analysis for the single fiber model also resulted in the average thermal stresses 0.11 MPa in tension for the fiber and 0.10 MPa in compression for the coating. Furthermore, the effective CTE of the single fiber model was 2.8×10^{-6}/°C for the finite element model and 2.7×10^{-6}/°C for the unit-cell model. The effective elastic modulus was 270 GPa and 272 GPa for the finite element

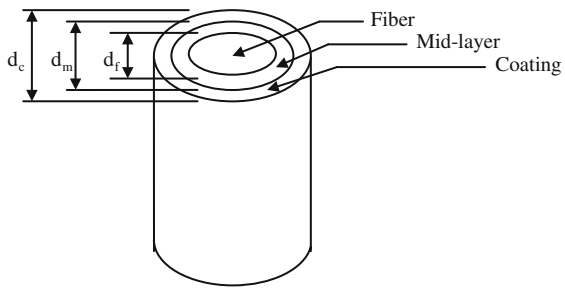

Fig. 7 Finite element model of a single fiber representative model

and unit-cell models, respectively. As a result, both analyses resulted in very close solutions.

When the interlayer did not have weak intra-layer bonding, thermal stresses in the fiber and coating materials increased significantly for the single fiber model. The finite element results showed that the reduction of thermal stresses in the coating and the fiber caused by the weakly bonded interlayer was proportional to the decrease of shear stresses at the interface. In other words, the thermal stresses were reduced approximately at the same ratio of the shear stress reduction in the weak interlayer.

The next study examined thermal stresses and effective thermomechanical properties of a plain weave composite using the unit-cell based multi-scale approach and the finite element analysis. The same material properties as used previously were considered with the volume fractions of the fiber, interlayer, and coating of 0.114, 0.419, and 0.467, respectively.

The finite element analysis with weak interlayer bonding resulted in the inplane elastic modulus of the plain-woven fabric composite of 170 GPa, inplane Poisson's ratio 0.16, and the inplane CTE 4.0×10^{-6}/°C, respectively. On the other hand, the present unit-cell based multi-scale model yielded the inplane elastic modulus 180 GPa, Poisson's ratio 0.17, and CTE 4.1×10^{-6}/°C, respectively. Hence, the two results agreed very well.

The thermal stress per unit temperature change in the fibers is plotted in Fig. 8. The plotted thermal stress is along the fiber orientation which is about 45° from the horizontal axis in the counter-clockwise direction. The plot shows some stress concentration due to abrupt bending of the fibers in the finite element model. However, the actual fibers have more gradual undulation so that the stress concentration may be neglected. In that regards, the thermal stress in the fibers of the finite element model is about 0.85 MPa at the undulated section. On the other hand, the thermal stress calculated from the unit-cell based multi-scale model gave 0.8 MPa for the same fiber section of the plain weave composite.

If the interlayer between the fiber and the coating is assumed to have perfect bonding, the thermal stress in the fiber increases as sketched in Fig. 9. The finite element analysis indicates approximately 1.2 MPa for the thermal stress in the fiber per unit temperature change. The unit-cell based multi-scale model also predicted 1.1 MPa for the thermal stress. Hence, both analyses yielded an excellent agreement. The weak interface reduced the fiber thermal stress by about 40%.

Furthermore, the thermal stress in the coating material agreed well between the finite element model and the multi-scale model. For example, as the fiber volume fraction increased to 0.4 while the interlayer and coating had volume fractions of 0.29 and 0.31, respectively, the thermal

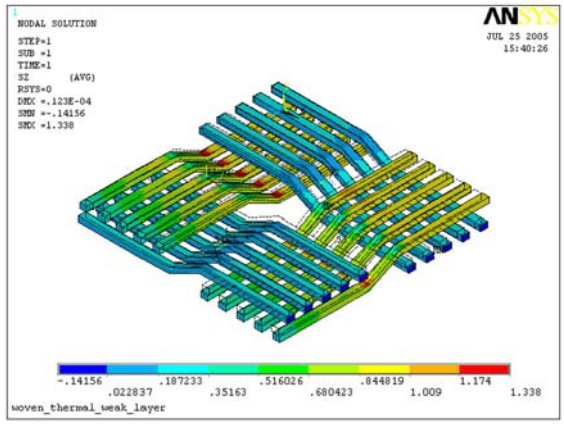

Fig. 8 Plot of thermal stresses in the fibers of a weak interlayer plain weave composite, along the fiber direction which is about 45° counter-clockwise from the horizontal axis

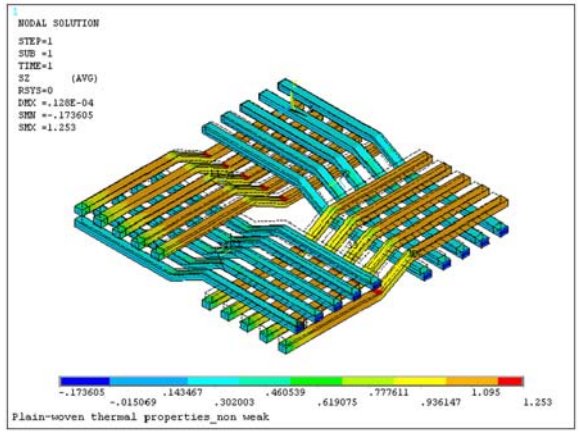

Fig. 9 Plot of thermal stresses in the fibers of a perfect interlayer plain weave composite, along the fiber direction which is about 45° counter-clockwise from the horizontal axis

stress in the coating was 0.64 MPa and 0.62 MPa for the finite element model and the multi-scale analysis model, respectively, per unit temperature change.

The final set of study investigates the effects of different material properties on the thermal stresses in the fibers and the coating materials. Figure 10 plots normalized thermal stresses in the fiber and the coating as each property changes independently while others held fixed. The figure shows that thermal stresses in the fiber and the coating vary linearly with the change of the CTE of either material. However, the thermal stress in the coating varies nonlinearly with the change of elastic modulus of either material. The fiber has a slightly nonlinear variation of the thermal stress as a function of the elastic modulus. Comparing the fiber and coating thermal stresses, the latter is more affected than the former by a property change. The CTE of the coating material has the largest effect on the thermal stresses in both the fiber and the

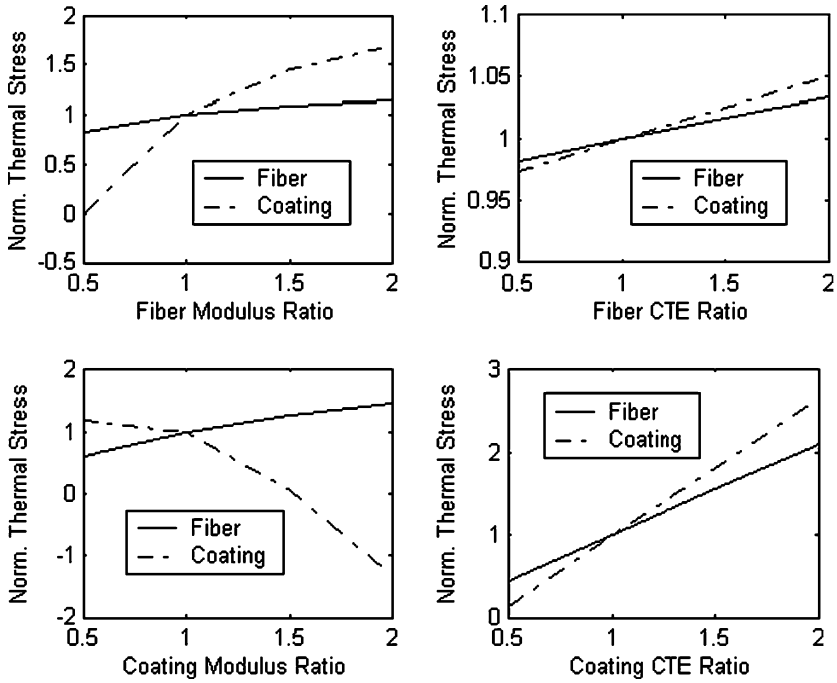

Fig. 10 Plot of normalized thermal stresses in the fiber and the coating as each property changes independently

coating while the CTE of the fiber material has the least effect on the thermal stresses. Generally, an increase of any material property results in a larger difference of the material properties between the fiber and the coating, and it increases the magnitude of the thermal stresses in both materials.

Conclusions

A multi-scale approach based on a series of unit-cell models was developed for a refractory, woven fabric composite, which is made of carbon fibers, a ceramic coating, and the weak interlayers between them. The approach computed micro-level thermal stresses occurring in the fibers and coating materials due to mismatch of CTE's between the two materials as well as the effective thermomechanical properties of a plain weave composite. In addition, detailed finite element models were developed and analyzed for evaluation of the unit-cell models. The finite element analyses modeled respective fibers, interlayers, and the coating materials discretely. Therefore, thermal stresses in each respective material could be calculated in the finite element analysis and compared to the unit-cell based results. Both results agreed well at the micro-scale and macro-scale level analysis, respectively.

The weak interlayer contributed significantly toward reduction of thermal stresses in the fiber and coating materials. Low thermal stress in the coating material was particularly important so that the coating layer did not crack and could continue to provide anti-oxidation protection to the carbon material. Consequently, the multi-scale model can be used for an optimal design of a refractory composite with diverse combinations of fiber and coating materials. Furthermore, the present model can be easily modified to various kinds of textile composites.

References

1. Tauchert TR, Hetnarski RB (1986) J. Thermal Stresses 9:1
2. Keene FW, Hetnarski RB (1990) J. Thermal Stresses 13:343
3. Ashida F, Tauchert TR (2003) Acta Mech 161:1
4. Barut A, Madenci E (2004) J. Thermal Stresses 27:1
5. Kwon YW, Burner JM (1997) Comput Struct 64:375
6. Aboudi J (1989) Appl Mech Rev 42:193
7. Sinha AK, Kokini K (1991) J. Thermal Stresses 14:1
8. Kwon YW, Kim C (1998) J Thermal Stresses 21:21
9. Kwon YW, Cho WM (2004) J Thermal Stresses 27:59
10. Kwon YW (1993) Composite Structures 25:187
11. Cox BN, Flanagan G (1997) NASA Contractor Report 4750